HAL open science

C-2p Spin-Polarizations along with Two Mechanisms in Extended Carbon Multilayers: Insight from First Principles

Samir Matar

▶ To cite this version:

Samir Matar. C-2p Spin-Polarizations along with Two Mechanisms in Extended Carbon Multilayers: Insight from First Principles. Condensed Matter, 2020, 5 (3), 48 (10 p.). 10.3390/condmat5030048 . hal-02943249

HAL Id: hal-02943249

https://hal.science/hal-02943249v1

Submitted on 21 Jan 2022

HAL is a multi-disciplinary open access archive for the deposit and dissemination of scientific research documents, whether they are published or not. The documents may come from teaching and research institutions in France or abroad, or from public or private research centers.

L'archive ouverte pluridisciplinaire **HAL**, est destinée au dépôt et à la diffusion de documents scientifiques de niveau recherche, publiés ou non, émanant des établissements d'enseignement et de recherche français ou étrangers, des laboratoires publics ou privés.

condensed matter

MDPI

Article

C-2*p* Spin-Polarizations along with Two Mechanisms in Extended Carbon Multilayers: Insight from First Principles

Samir F. Matar [1,2]

[1] Lebanese German University, Sahel-Alma, Jounieh P.O.BOX 206, Lebanon; s.matar@lgu.edu.lb or abouliess@gmail.com

[2] Formerly at University of Bordeaux, ICMCB–CNRS, 33600 Pessac, France

Received: 8 June 2020; Accepted: 17 July 2020; Published: 22 July 2020

Abstract: From density functional theory investigations helped with crystal chemistry rationale, single-atom C, embedded in layered hexagonal CC'_n (n = 6, 12 and 18) networks, is stable in a magnetic state with M(C) = 2 μ_B. The examined compositions, all inscribed within the P6/mmm space group are characterized as increasingly cohesive with n, figuring mono-, bi- and tri-layered honeycomb-like C′6 networks respectively. The spin projected total density of states shows a closely half-metallic behavior with a gap at minority spins (↓) and metallic majority spins (↑). Such results together with the large C-C intersite separation and the integer 2 μ_B magnetization, let us propose an intra-band mechanism of magnetic moment onset on carbon 2*p* states. Support is provided from complementary calculations assuming a $C_2C'_{12}$ structure with planar 2C with d(C-C) = 2.46 Å resulting into a lowering of the magnetization down to the 0.985 μ_B/C atom and a ferromagnetic order arising from interband spin polarization on C where one nonbonding spin polarizes whereas the other is involved with the bonding with the other carbon. Illustration of proofs is provided with the magnetic charge density projected onto the different atoms, showing its prevalence around C, contrary to the C'_n (C′6 layers), as well as electron localization function ELF.

Keywords: interband magnetism; intraband magnetism; carbon honeycomb; DFT; magnetic charge density; ELF; DOS

1. Introduction and Context

Unpaired electrons in outer shells of atoms let identify a paramagnetic behavior with no parallel alignment of spins. This is opposed to diamagnetic atoms where all electrons are paired such as in magnesium with Mg($3s^2$). Carbon, as an isolated element is paramagnetic C($2s^2$, $2p^2$) with 2 unpaired p-electrons. In fact, such a configuration is seldom encountered in chemical systems, because carbon and its neighbors combine through pairing their respective electrons to form bonds. In paramagnetic elements, a lowering of the energy occurs when the electron spins become parallel (↑,↑) and in certain cases, below a critical temperature called the Curie temperature T_C, an ordering of the spins occurs adding them up constructively and leading to a long-range ferromagnetic state. Regarding the highest occupied valence states of the 1st-period transition metals, three ferromagnetic metals are found: Fe($4s^2$, $3d^6$) with M = 2.2 μ_B, Co($4s^2$, $3d^7$) with M = 1.7 μ_B and Ni($4s^2$, $3d^8$) with M = 0.6 μ_B; all of them having unpaired d electrons and behaving as paramagnets above T_C. A close inspection is obtained from band structure calculations considering firstly a non-spin-polarized state (NSP). The d states show a significant localization illustrated by a high density of states (DOS) at the Fermi level E_F: $n(E_F)$, signaling the instability of such a spin degenerate configuration [1]. Upon carrying out further spin-polarized SP calculations accounting for two spin channels (majority spins ↑, and minority spins

↓), magnetic moments develop on the atoms. The designation of 'majority' and 'minority' arises from the fact that the former has a larger electron population because it is energy down-shifted oppositely to the minority spins DOS, which are energy up-shifted (cf. Figure 4). Such properties are quantified from the quantum density functional theory DFT [2,3]. In the 2nd and 3rd transition metal periods, the broadening of the 4d-and 5d bands hinders localization of the d states and hence the onset of magnetic polarization; but under certain crystal structure conditions, a narrowing of the bands may occur such as for the 3rd period iridium in a structure characterized by isolated *IrO6* octahedra within $Ca^{II}{}_4Ir^{IV}O_6$ and M(Ir)= 0.5 μ_B [4].

Then, in the 1st period ferromagnetic metals, the magnetic moment is of inter-band nature, meaning that it is mediated by the electron gas (s-like), i.e., in a "d ... s ... d"-like bridging and the magnetic moments are not integers as shown above. To some extent, uranium presents an intermediate situation where U 5f band, less narrow than rare-earth 4f one, behaves like a transition metal's d band [5].

Another kind of magnetism occurs for rare-earth gadolinium metal, characterized by half-filled 4f shell, i.e., with seven electrons, which all polarize to provide a high magnetic moment of 7 μ_B. Gd is a ferromagnet with T_C close to room temperature. Here, oppositely to Fe, Co and Ni, the magnetic polarization is of intra-(4f)band nature, i.e., without calling for the mediation of itinerant s electrons. The underlying effect is that 4f states are localized in a narrow band in the atomic state and they keep this behavior in the periodic organized solid.

Consequently, the elements with outer shells having unsaturated occupations as *n*d and 4f (above examples) are likely to lead to inter- and intraband spin polarization respectively, provided the conditions of sufficient band localization be met in the crystal environment.

Note that regarding *p*-elements magnetism, ordered magnetic moments were identified in hexaborides AEB_6 (AE = Ca, Sr) [6] as well as in CdS doped with the main group elements [7].

Focusing on carbon herein, one is presented with two possible situations regarding the onset of magnetization through:

i. Keeping an isolated atomic behavior—as for Gd (4f)—characterized by two unpaired carbon *p* electrons in an appropriate crystal–chemical host, and leading eventually to their polarization and the expectation of M(C) = 2 μ_B. We assess this within an intraband spin polarization mechanism;
ii. Checking for the hypothesis of interband spin polarization mechanism by involving two carbon neighbors at a distance which allows electronic interactions between them. The subsequent bonding involves a spin pairing and a loss of the magnetization magnitude. The expectation is a magnitude of M(C) close to 1 μ_B.

Along with these two hypotheses, and based on the DFT calculation of energies and magnetic configurations, the paper presents results and assessments of the two mechanisms in new carbon-based model multilayered systems. While the present investigation is of theoretical scope, feasibility aspects find support from experimental preparation of multilayered graphene/graphite sheets [8].

2. Brief Presentation of the Computational Methodology

Within the DFT, the optimization of the candidate structures (the atomic positions and the lattice parameters) is needed in the first place to identify the minimum energy configuration. The plane wave Vienna ab initio simulation package (VASP) package [9,10] was used with its implementation of the projector augmented wave (PAW) method [10,11]. The DFT exchange-correlation effects were accounted for with the generalized gradient approximation (GGA) scheme [12]. A conjugate-gradient algorithm [13] was used to relax the atom positions of the different compositions into the ground-state structure. Structural parameters were considered as fully minimized when forces on the atoms were less than 0.02 eV/Å and the stress components were below 0.003 eV/Å. A tetrahedron method [14] was applied for geometry relaxation and total energy calculations. The integrals within the reciprocal space

(Brillouin zone BZ) were approximated using a special **k**-point sampling [15]. The calculations were converged at an energy cut-off of 400 eV for all compounds. The **k**-mesh integration was carried out with increasing BZ precision over successive calculations for best convergence and relaxation to zero strains. Calculations were systematically carried out considering both non-spin-polarized (NSP) and spin-polarized (SP)–magnetic configurations.

Properties related with electron localization are obtained from real space analysis of electron localization function (ELF) according to Becke and Edgecomb [16] as initially devised for Hartree–Fock calculations then adapted to DFT methods as based on the kinetic energy in which the Pauli exclusion principle is included by Savin et al. [17]: ELF = $(1 + \chi_\sigma{}^2)^{-1}$ with $0 \leq$ ELF ≤ 1, i.e., ELF is a normalized function. In this expression the ratio $\chi_\sigma = D_\sigma/D_\sigma{}^0$, where $D_\sigma = \tau_\sigma - \frac{1}{4}(\nabla\rho_\sigma)^2/\rho_\sigma$ and $D_\sigma{}^0 = 3/5\ (6\pi^2)^{2/3}\rho_\sigma{}^{5/3}$ correspond respectively to a measure of Pauli repulsion (D_σ) of the actual system and to the free electron gas repulsion ($D_\sigma{}^0$) and τ_σ is the kinetic energy density. ELF is a normalized function with $0 \leq$ ELF ≤ 1, ranging from 0 for no localization to 1 for full localization; magnitudes 1/2 correspond to free-electron like localization.

3. Results and Discussion

3.1. Geometry Optimization and Energy-Dependent Results

3.1.1. CC'_n (n = 6, 12 and 18)

Honeycomb carbon networks were identified in the lithium graphitic anode materials LiC_6 and LiC_{12} [18] with the *P6/mmm* space group. Full geometry relaxations were carried out assuming NSP and SP configurations. The results are given in Table 1b. The respective structures transposed to CC'_6 and CC'_{12} are shown in Figure 1a,b. In both compounds, the SP configuration has lower energy than the NSP and the cohesive energies obtained from subtracting the atomic C contributions are negative with the same trends of larger stability of SP. Comparing CC'_6 to CC'_{12}, the latter exhibits a larger cohesive energy letting propose that two C′6 layered compounds are more favorable. One can also note that the magnetization of M = 2 μ_B remains the same in the two compounds, due to the full polarization of carbon two *p* electrons. Regarding the crystal parameters, the onset of spin polarization causes a large increase of the hexagonal *c/a* ratio while few changes can be observed for the hexagonal *a* lattice constant as well as the C′ positions, which are mainly determined by the rigid C′6 network. In both stoichiometries, d(C′-C′) changes little, with 1.4 Å and almost unchanged by the spin state. Such trends and observations needed to be further confirmed with a structure comprising three C′6 layers with the formulation CC'''_{18}, with C at the origin and the layers at C′ and C″. The obtained structure within the same space group is shown in Figure 1c and the geometry optimized parameters and energies explicated in Table 1(c). Indeed the trend of stabilization through multilayered stoichiometry is confirmed with similar trends of lattice parameters and an increase of hexagonal *c/a* ratio always larger in SP than with the increase of the $E_{coh.}$ magnitude to −1.69 eV, i.e., versus $E_{coh.}$ (CC'_{12}) = −1.518 eV and $E_{coh.}$ (CC'_6) = −1.021 eV (SP values, per C atom). Additionally, the SP configuration is more cohesive than NSP and the magnitude of the magnetic moment on C is 1.98 μ_B, close to the saturation moment of 2 μ_B.

A most relevant result from the calculations is the integer 2 μ_B magnitude of corner C in all structures. The C-C separation is large and amounts to the *a* lattice constant magnitude, which is systematically larger than 4 Å, suggesting an isolated character and a development of onsite magnetic moment through intraband spin polarization.

3.1.2. $C_2C'_{12}$

Support of the above hypothesis was needed with a structure accounting for two neighboring carbon atoms that would magnetically polarize through an inter-band mechanism.

Figure 1d shows $C_2C'_{12}$ structure based on the *P6/mmm* space group and where C belongs to a two-fold Wyckoff position, i.e., at 1/3, 2/3, 1/2 and 2/3, 1/3, 1/2. After full geometry relaxation, the C-C distance was 2.46 Å. The results show SP as the ground state with, however, a cohesive energy of −1.22 eV/at, smaller than the cohesive energy of CC'_{12} of −1.518 eV. The remarkable result is now the lowering of the magnitude of magnetization, which amounts to 1.97 μ_B for the two carbon atoms, i.e., 0.985 μ_B/C atom. The long-range magnetic order is ferromagnetic. Further antiferromagnetic calculations imposing two magnetic substructures, one labeled as SPIN UP and the other as SPIN-DOWN, i.e., C↑ . . . C↓ as well as all the C′ atoms. At self-consistent convergence, a raise of the energy was noted and the system becomes less cohesive.

One can then assume that the loss of magnetization magnitude is due to spin pairing through the bonding between the two carbon atoms, leaving one nonbonding spin polarizing along the *c* hexagonal direction. The mechanism of spin polarization is then suggested to be of an interband nature.

Table 1. Calculated results for lattice parameters with distances given in Å and energies in eV. Space group *P6/mmm* N°191. In the three CC'_n crystal structures, C is at (1*a*) (0,0,0) and in $C_2C'_{12}$, C at (2*c*) 1/3, 2/3, 0 (cf. Figure 1). Atomic energy: E_C = −7.11 eV.

(a). CC'_6.		
Magn. Config.	NSP	SP
a	4.285	4.272
c/a	0.933	1.183
d(C′-C′)	1.41–1.43	1.42-1.43
C′(6k) x, 0, $\frac{1}{2}$	0.335	0.333
Tot. Energy	56.23	−56.91
Ecoh. /at.	−0.932	−1.021
M (μ_B)	-	2.01
(b). CC′12.		
Magn. Config.	NSP	SP
a	4.278	4.265
c/a	1.820	2.060
d(C′-C′)	1.42–1.43	1.42–1.43
C′(12n) x, 0, z	0.334/0.280	0.333/0.297
Tot. Energy	111.46	−112.16
Ecoh. /at.	−1.464	−1.518
M (μ_B)	-	2.01
(c). CC‴18 (CC′12C″6).		
Magn. Config.	NSP	SP
a	4.275	4.265
c/a	2.57	2.68
d(C′-C′)(C″-C″)	1.41–1.42	1.41–1.42
C′(12n) x, 0, z	0.334/0.183	0.333/0.196
C″(6k) x, 0, $\frac{1}{2}$	0.333	0.334
Tot. Energy	166.57	−167.22
Ecoh. /at.	−1.657	−1.691
M (μ_B)	-	1.980
(d). C2C′12.		
Magn. Config.	NSP	SP
a	4.220	4.230
c/a	2.238	2.458
d(C′-C′)	1.41	1.41
C′(12n) x, 0, z	0.333/0.319	0.333/0.308
Tot. Energy	116.46	−116.60
Ecoh. /at.	−1.20	−1.22
M (μ_B)	-	1.97 (2 C)

3.2. Magnetic Charge Density

The above results need to be supported by the magnetic charge densities on the different atomic constituents on one hand and with a projection of the electron localization on the other hand.

The magnetic charge density corresponds to the density difference between majority spins (↑) and minority spins (↓). Figure 1 shows the magnetic charge density around the atoms with the rainbow colored spheres. One can see in Figure 1b,d the difference occurring for nearest neighboring two successive Fe's, i.e., with d(Fe-Fe) = *a* lattice constant in CC'_6 (Figure 1b), which amounted to more than 4 Å. Oppositely, in $C_2C'_{12}$ (Figure 1d), the in-plane two neighboring Fe were at a 2.46 Å smaller separation. For the C′ and C″ atoms belonging to the C'_6 layers, there were no magnetic charge densities around them since the difference of population ↑-↓ is zero. While this is expected, it is interesting to note the difference of shapes between the spheric-like volume for the isolated C in Figure 1 a–c versus the elongated shape along with the c direction in Figure 1d.

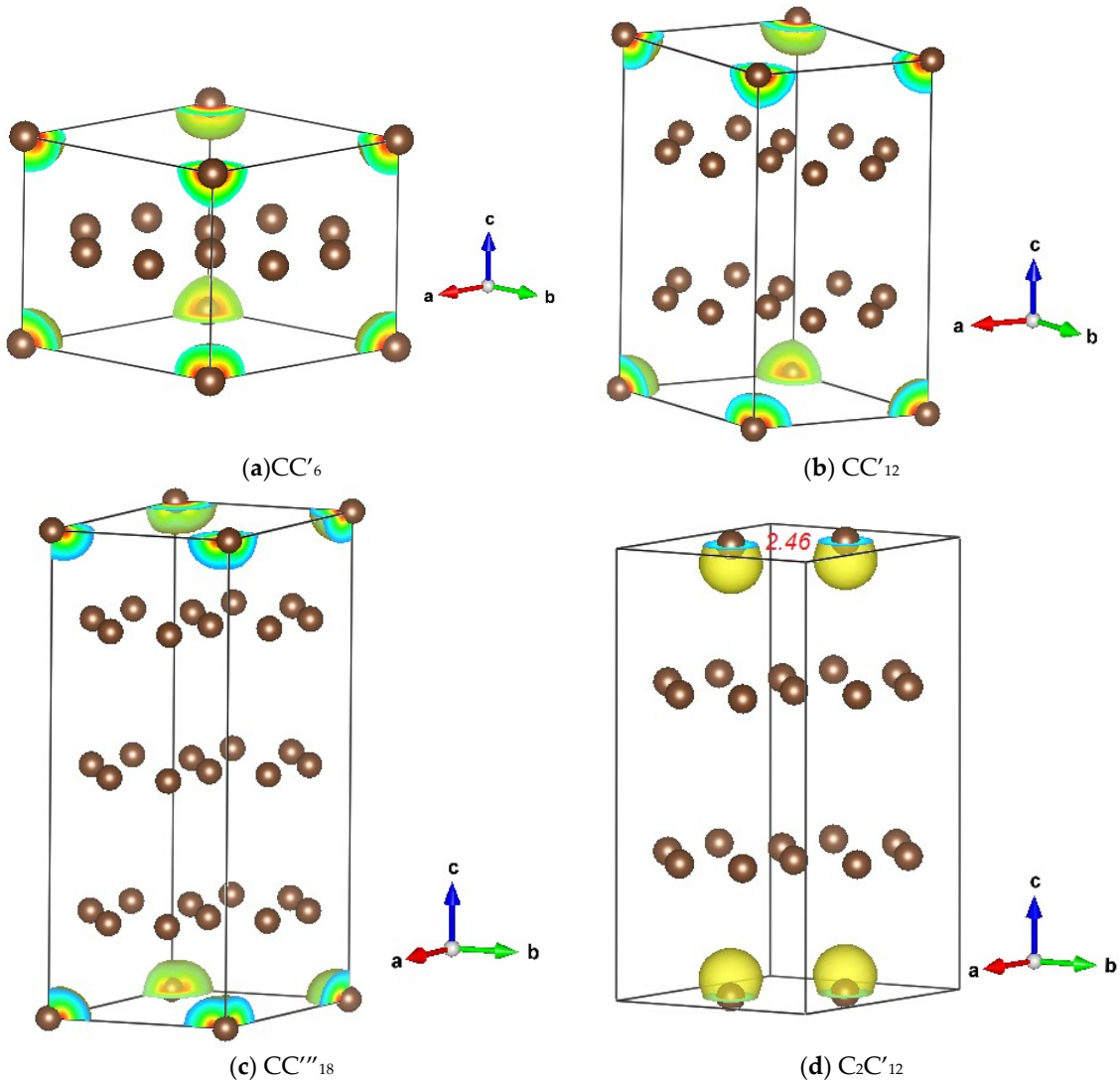

(**a**)CC'_6 (**b**) CC'_{12}

(**c**) CC'''_{18} (**d**) $C_2C'_{12}$

Figure 1. (**a**–**c**) Sketches of the crystal structures of mono, bi- and tri-layered chemical systems. Carbon atoms at the corners are represented with magnetic charge density exhibited by the colored envelops, specifically showing that magnetic polarization occurs only on them with M = 2 μ_B. (**d**) $C_2C'_{12}$ structure showing the prevailing interband spin polarization with a lowering to 1 μ_B per carbon due to the presence of two C neighbors characterized by significant charge localization between them with an itinerant character from ELF at Figure 2e.

3.3. Electron Localization Function ELF

The ELF are shown in Figure 2. The color scheme is as follows: blue for ELF = 0 (no localization); red color for full localization with ELF = 1 and green color for ELF = 1/2, corresponding to a free electron-like behavior. Firstly in Figure 2a we show the ELF of a C′ layer in 2 × 2 × 1 projection where the red zones of strong localization allow depicting the C′6 (C″6) rings forming such layers. There are no blue zones pointing to no electron localization and the layer is similar to a graphitic one letting it suggest a semi-conducting like behavior for the layer. Focusing on the basal planes, Figure 2b–d exhibits blue zones of no localization between the C sites thus supporting their isolated character electronically and magnetically, with d(C-C)~a_{hex}. Oppositely, in Figure 2e relevant to $C_2C'_{12}$, the two C atoms are in the basal plane at a distance of 2.46 Å and there is a significant green zone of free electron-like character between the two atoms. Then the ELF projections provide further illustration of the different magnetic behaviors observed, i.e., intraband *versus* interband magnetic polarizations.

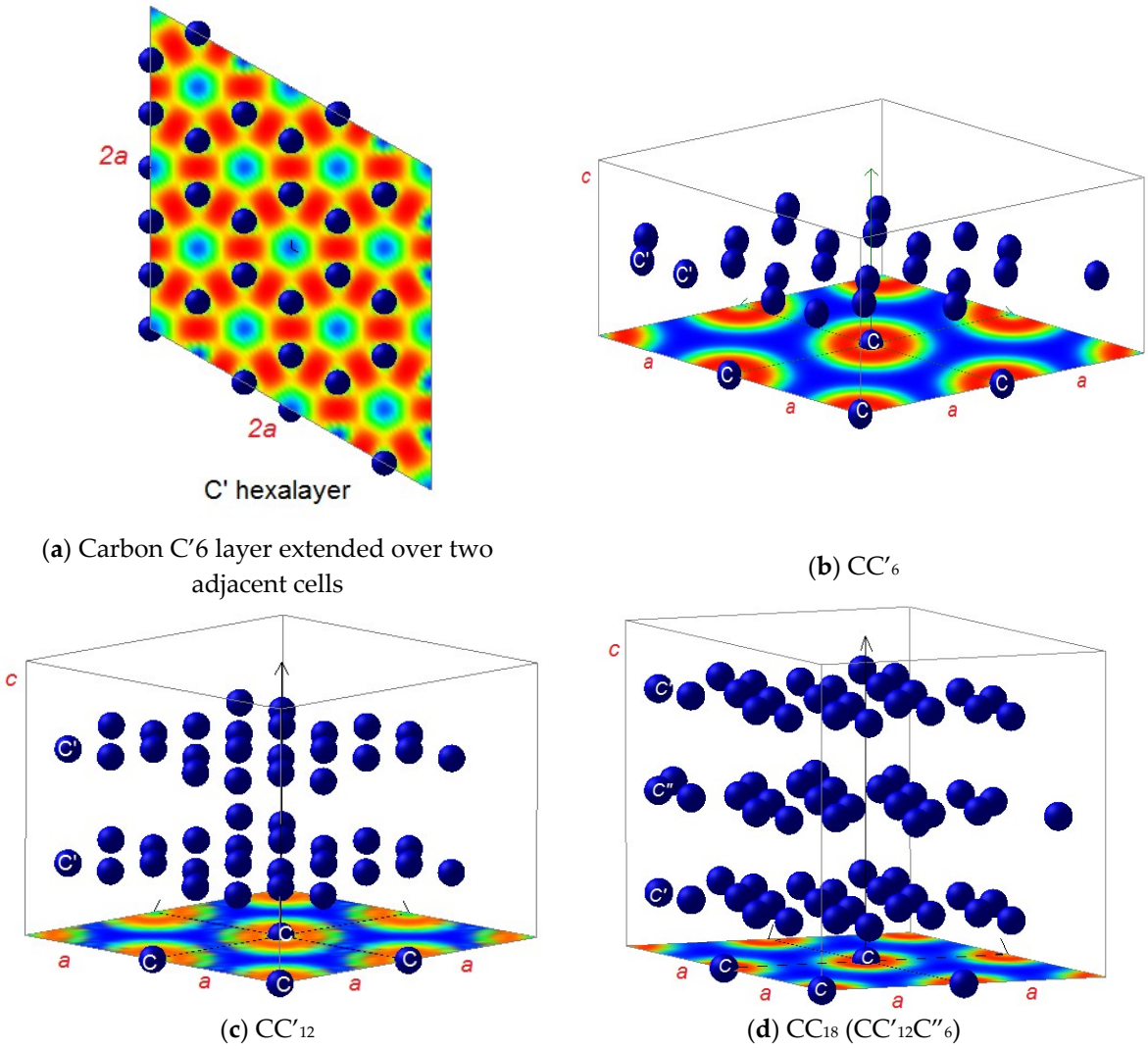

(**a**) Carbon C′6 layer extended over two adjacent cells

(**b**) CC'_6

(**c**) CC'_{12}

(**d**) CC_{18} ($CC'_{12}C''_6$)

Figure 2. *Cont.*

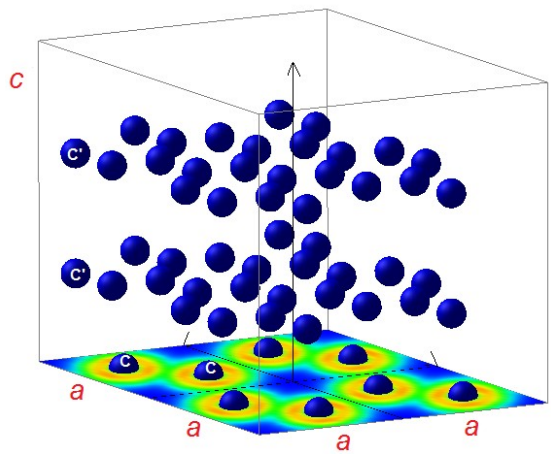

(**e**) $C_2C'_{12}$

Figure 2. Electron localization function (ELF) with a 2 × 2 × 1 projection. (**a**) C'_6 plane; (**b**–**d**) ELF slices crossing the basal plane containing C and (**e**) ELF crossing the plane containing two adjacent C atoms. Notice the free electron-like behavior (green) between the C atoms stressing the inter-band spin-polarization mechanism in $C_2C'_{12}$ (**e**).

3.4. Analysis of the Electronic Density of States

Considering non-spin-polarized configurations (NSPs), Figure 3 shows the orbital projected DOS of C typically observed in the CC'_n stoichiometries. There are two kinds of partial DOS: an intense sharp peak and a slightly broader one, both centered on the Fermi level (zero of energy along the *x*-axis). In the *P6/mmm* space group, the corresponding point group is D_{6h}, which leads to the observed split in two manifolds A_{1u} and E_{2u} for p_z and $p_{x,y}$ respectively. The high DOS at E_F is a signal of instability in such spin degenerate configuration.

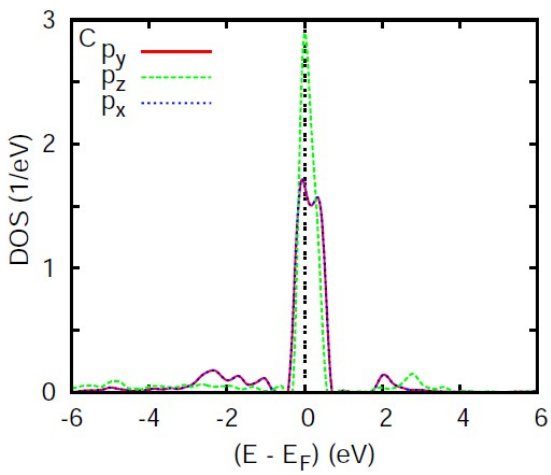

Figure 3. Density of states (DOS) of the three carbon *p* orbitals in non-spin-polarized configuration (NSP) calculations of CC'_n. The splitting in D_{6h} point group of *P6/mmm* space group leads to two manifolds of C-2*p*: A_{1u} and E_{2u} for p_z and $p_{x,y}$ resp. The high DOS at E_F is a signal of instability in such a spin degenerate configuration.

From the subsequent SP calculations, the total DOS were plotted for majority spins (↑) and minority spins (↓) in Figure 4. The difference between the two populations provides a magnetic moment. The energy position of the Fermi level is indicated and shown to be at a minimum of minority spins $n(E_F \downarrow)$ observed for all three CC'_n stoichiometries, whence the integer 2 μ_B/C atom and the half-metallic ferromagnet character.

Different features appear for the last panel corresponding to the $C_2C'_{12}$ SP DOS, which show less energy shift difference between the two spin DOS and broader and less shaped DOS. Additionally, one can notice the absence of a trough at E_F for either $n(E_F)$ ↑ or ↓ with and a rather metallic-like character. These results are further illustrations of the intraband magnetism on C with an integer moment of 2 μ_B v/s interband magnetism, with a non-integer moment on carbon lower than 1 μ_B. The first mechanism being illustrated by the half-metallic ferromagnetic behavior of the SP-DOS, with a deep minimum as shown in Figure 4b for the minority spins (↓) at E_F; oppositely to the continuing, non-interrupted DOS in both spin channels, ↑ and ↓ with no trough at E_F (Figure 4d).

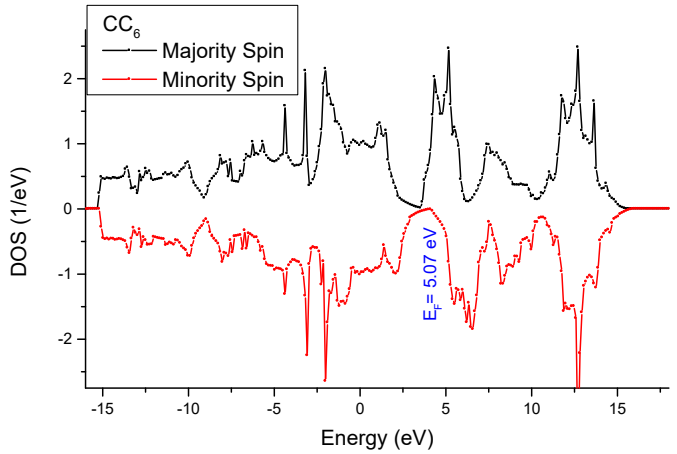

(a)

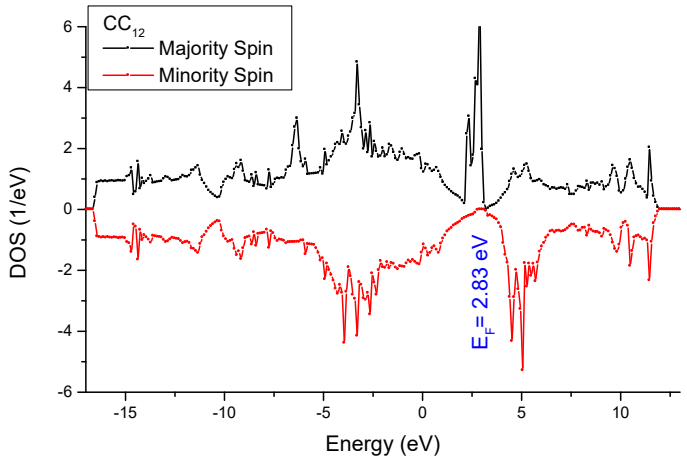

(b)

Figure 4. *Cont.*

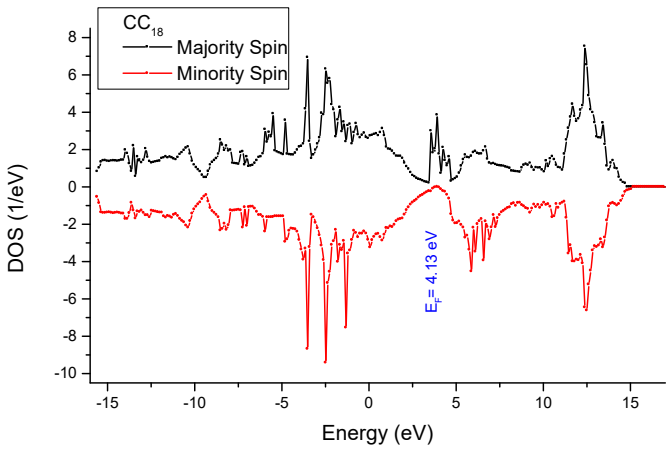

(c)

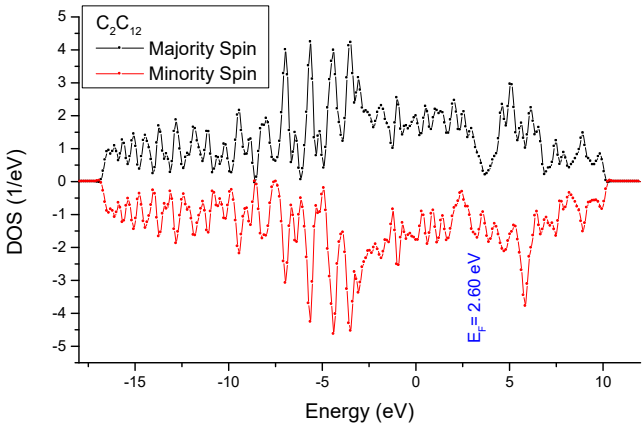

(d)

Figure 4. Spin projected total DOS of the CC′$_n$ (n = 6, 12 and 18) and $C_2C'_{12}$ stoichiometries. (**a**) CC′$_6$, (**b**) CC′$_{12}$, (**c**) CC′$_{18}$, (**d**) $C_2C'_{12}$.

4. Conclusions

We have shown that magnetically polarized carbon was increasingly stabilized upon considering hosting multilayer new CC′$_n$ (n = 6, 12 and 18) stoichiometries within the hexagonal *P6/mmm* space group. The occurrence for C of a particular mechanism for the onset of magnetization was highlighted and identified as being of an intra-band type featuring an integer magnetization of 2 μ_B due to the large separation between nearest neighbor atoms. Considering further a stoichiometry with 2 C closer neighbors in model $C_2C'_{12}$, an interband spin polarization mechanism was identified and illustrated with an electron localization projection showing a free electron-like localization between the two atoms. The magnetization drops then to less than 1 μ_B /at. due to the pairing of one spin to ensure for the interaction between the two in-plane carbon atoms. It is worth mentioning at this point that the layered-like host structures proposed herein are unique in supporting magnetic polarizations (inter- and intra-); that is, with respect to $LaNi_5$-type or AlB_2-type, both known in the *P6/mmm* N°191 space group, but presenting less extended networks.

While further investigations are needed to clearly identify the magnitude of the Curie order temperature knowing the DFT calculations are zero-temperature, efforts for preparing such multilayer new stoichiometries in view [8]. Our results are also supported by recently identified observation of critical magnetic behavior in 2D carbon based composites by Shukla [19].

Funding: This research received no external funding.

Acknowledgments: We used VESTA software for the structure and charge density sketches [20]. Computations were carried out on Xeon workstations of C^2M^2S (Computer Center for Materials and Molecular Sciences) of the Lebanese German University.

Conflicts of Interest: The author declares no conflict of interest.

References

1. Mohn, P. *Magnetism in the Solid State—An Introduction*; Springer Series in Solid-State Sciences; Springer: Heidelberg, Germany, 2003.
2. Hohenberg, P.; Kohn, W. Inhomogeneous Electron Gas. *Phys. Rev.* **1964**, *136*, B864–B871. [CrossRef]
3. Kohn, W.; Sham, L.J. Self-Consistent Equations Including Exchange and Correlation Effects. *Phys. Rev.* **1965**, *140*, A1133–A1138. [CrossRef]
4. Matar, S.F.; Etourneau, J. $(CaO)_nIrO_2$ (n = 1, 2, 4) family: Chemical scissors effects of CaO on structural characteristics correlated to physical properties. Ab initio study. *J. Solid State Chem.* **2017**, *255*, 82–88. [CrossRef]
5. Matar, S.F.; Eyert, V.; Mavromaras, A.; Najm, S.; Chevalier, B.; Etourneau, J. Chemical bonding and magnetism in the ternary germanides UT_2Ge_2 (T = 3d transition metal) from local spin density functional calculations. *J. Magn. Magn. Mater.* **1997**, *174*, 219–235. [CrossRef]
6. Dorneles, L.S.; Venkatesan, M.; Moliner, M.; Lunney, J.G.; Coey, J.M.D. Magnetism in thin films of CaB_6 and SrB_6. *Appl. Phys. Lett.* **2004**, *85*, 6377–6379. [CrossRef]
7. Bedolla, P.O.; Gruber, C.; Mohn, P.; Redinger, J. p-electron magnetism in CdS doped with main group elements p-electron magnetism in CdS doped with main group elements. *J. Phys. Condens. Matter.* **2012**, *24*, 476002–476005. [CrossRef] [PubMed]
8. Tatami, A.; Tachibana, M.; Yagi, T.; Murakami, M. Preparation of multilayer graphene sheets and their applications for particle accelerators. *AIP Conf. Proc.* **2018**, *1962*, 030005. [CrossRef]
9. Kresse, G.; Furthmüller, J. Efficiency of ab-initio total-energy calculations for metals and semiconductors using a plane-wave basis set. *Phys. Rev. B Condens. Matter Mater. Phys.* **1996**, *54*, 11169–11186. [CrossRef] [PubMed]
10. Kresse, G.; Joubert, J. From ultrasoft pseudopotentials to the projector augmented wave. *Phys. Rev. B Condens. Matter Mater. Phys.* **1999**, *59*, 1758–1775. [CrossRef]
11. Blöchl, P.E. The projected augmented wave method. *Phys. Rev. B Condens. Matter Mater. Phys.* **1994**, *50*, 17953–17979. [CrossRef] [PubMed]
12. Perdew, J.; Burke, K.; Ernzerhof, M. The Generalized Gradient Approximation Made Simple. *Phys. Rev. Lett.* **1996**, *77*, 3865–3868. [CrossRef] [PubMed]
13. Press, W.H.; Flannery, B.P.; Teukolsky, S.A.; Vetterling, W.T. *Numerical Recipes*; Cambridge University Press: New York, NY, USA, 1986.
14. Blöchl, P.E.; Jepsen, O.; Anderson, O.K. Improved tetrahedron method for Brillouin-zone integrations. *Phys. Rev. B* **1994**, *49*, 16223. [CrossRef] [PubMed]
15. Monkhorst, H.J.; Pack, J.D. Special k-points for Brillouin Zone integration. *Phys. Rev. B* **1976**, *13*, 5188. [CrossRef]
16. Becke, D.; Edgecombe, K.E. A simple measure of electron localization. *J. Chem. Phys.* **1990**, *92*, 5397–5401. [CrossRef]
17. Savin, A.; Jepsen, O.; Flad, J.; Andersen, K.O.; Preuss, H.; von Schnering, H.G. The ELF perspective of chemical bonding. *Angew. Chem. Int. Ed. Engl.* **1992**, *31*, 187–191. [CrossRef]
18. Dolotko, O.; Senyshyn, A.; Mühlbauer, M.J.; Nikolowski, K.; Ehrenberg, H. Understanding structural changes in NMC Li-ion cells by in situ neutron diffraction. *J. Power Sources* **2014**, *255*, 197–200. [CrossRef]
19. Shukla, V. Observation of critical magnetic behavior in 2D carbon based composites. *Nanoscale Adv.* **2020**, *2*, 962. [CrossRef]
20. Momma, K.; Izumi, F. VESTA 3 for three-dimensional visualization of crystal, volumetric and morphology data. *J. Appl. Crystallogr.* **2001**, *44*, 1272. [CrossRef]

© 2020 by the author. Licensee MDPI, Basel, Switzerland. This article is an open access article distributed under the terms and conditions of the Creative Commons Attribution (CC BY) license (http://creativecommons.org/licenses/by/4.0/).